Supporting Information for

Rocking-Chair Configuration in Ultrathin Lithium Vanadate-Graphene Hybrid Nanosheets for Electrical Modulation

Haiou Zhu[1], Xinming Qin[2], Xu Sun[1], Wensheng Yan[3], Jinlong Yang[2*] and Yi Xie[1*]

[1]Division of Nanomaterials and Nanochemistry, Hefei National Laboratory for Physical Sciences at the Microscale, University of Science and Technology of China, Hefei, Anhui, 230026, P. R. China

[2]Theoretical and Computational Sciences, Hefei National Laboratory for Physical Sciences at Microscale, University of Science & Technology of China, Hefei, Anhui, 230026, P. R. China

[3]National Synchrotron Radiation Laboratory, University of Science and Technology of China, Hefei, Anhui 230029, P.R. China

This supporting information includes:

1. **Fig.** S1-S12
2. Supplementary references

S1. The crystallographic information of $Li_{1.2}V_{3.34}O_{7.34}•2H_2O$ (LiVO) and LiVO-graphene

$Li_{1.2}V_{3.34}O_{7.34}•2H_2O$ (abbreviated as LiVO thereafter) is a tetragonal crystal with layered structure which forms a layered stacking along the 001 direction with the H_2O located between its layers, the cell parameters a and c is 3.705Å and 15.804Å, respectively, with space group I 4/mmm. The building block of the layered structure is the tetragonal pyramid and each adjacent pyramid is rendered in opposite direction. The lithium ions resided between the vanadium oxide sheets being bonded by the lattice oxygen and the water oxygen.

The vanadium oxide sheets are planar, and the vanadium oxide have identical coordination, the lithium ions reside between the layers can be reversibly intercalated/extracted from the vanadium oxide layers, making LiVO candidate for the cathode of lithium ion battery. Graphene is likely be intercalated into the host LiVO lamellar, since graphene has a layered structure similar to LiVO. Weak van der Waals interlayer interactions are present among the layers, bringing the exfoliative characteristic to this compound.[1,2] The schematic diagram of the structure of $Li_{1.2}V_{3.34}O_{7.34}•2H_2O$. (LiVO) is shown in Figure S1a.

When graphene was intercalated into the LiVO framework, the interlayer d-spacing of LiVO increased from 7.9Å to 12.5Å , with Δd of 4.6Å after graphene intercalation. The suggested schematic diagram of the structure of new LiVO framework after graphene intercalation was shown in Figure S1b, and the simulated XRD diffraction pattern of which was shown in Figure 1c. The simulated XRD pattern of new LiVO framework matches well with the new peaks arising after intercalation in the measured XRD pattern of LiVO-graphene in Figure 1c, indicating that the suggested schematic structure is coincident with the actual situation.

The schematic diagram of the structure of LiVO-graphene is shown in Figure S1c, with a graphene layer intercalated into the new LiVO framework.

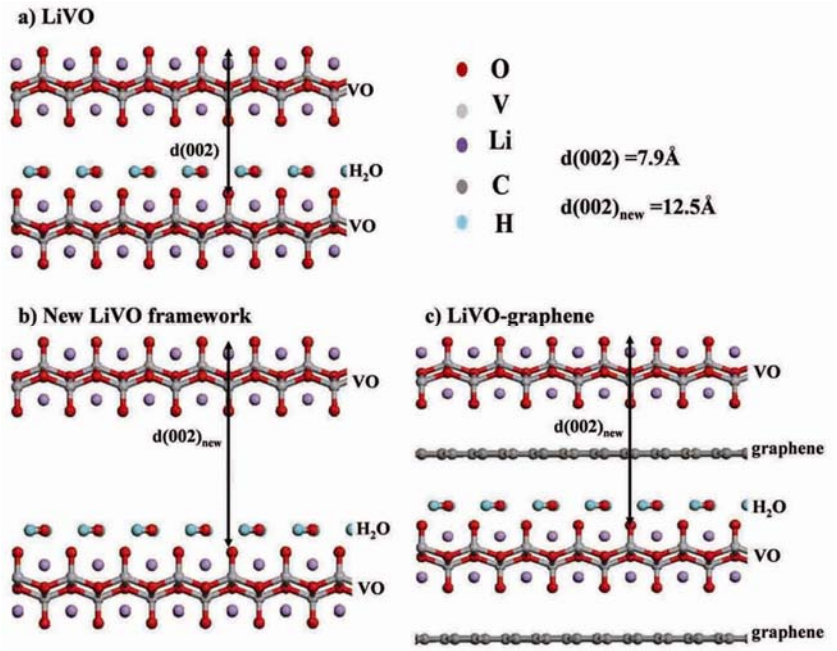

Figure S1. The schematic diagram of the structure of a) $Li_{1.2}V_{3.34}O_{7.34}$•$2H_2O$ (LiVO) (the view of the planar perpendicular to the LiVO sheets-(001)), b) new LiVO framework and c) LiVO-graphene.

S2. The XPS survey spectra of the as-prepared pure LiVO and LiVO-graphene

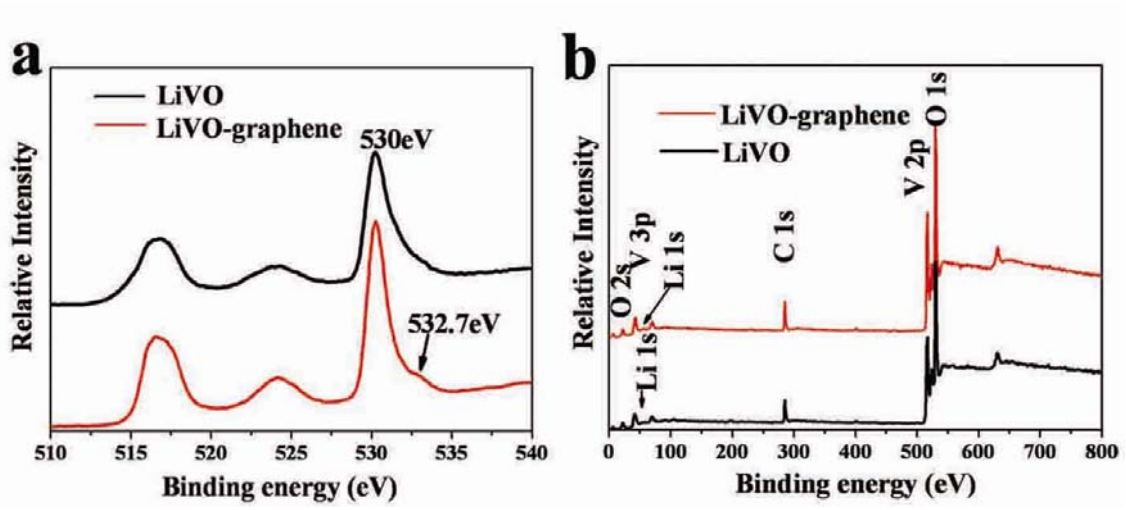

Figure S2. XPS spectra of the pure LiVO and LiVO-graphene for a) V 2p region, and b) the survey spectra.

According to the high-resolution XPS spectra for V 2p region, the peak at 516.6eV can be assigned to V^{4+}, The peaks at about 525eV can

be assigned to the V 3d level. In the XPS spectrum of LiVO, the core level at 530eV with the dominant O amounts can be assigned to V-O bonding, while in the spectrum of LiVO-graphene, there was a new peak at 532.7eV appears and can be attributed to the C-O bonding,[3] which can be ascribed to surface functional groups of the graphene ring. Further chemical composition information was shown in the survey spectra comparison between LiVO and LiVO-graphene in Figure S2b, observed from the survey spectra, pure LiVO and LiVO-graphene samples are mainly consisted of vanadium, oxygen and lithium similarly, revealing that pure LiVO and LiVO-graphene have similar chemical composition. It has to be emphasized that the C1s peak at 284.8eV can not be indexed to C in graphene, for the C1s here is used to calibrate the binding-energy scale for XPS measurement with non-conducting specimens, and a binding energy of 284.8eV has been assumed for this purpose.

S3. The energy dispersive X-ray spectroscopy (EDS) spectra of LiVO-graphene nanosheets

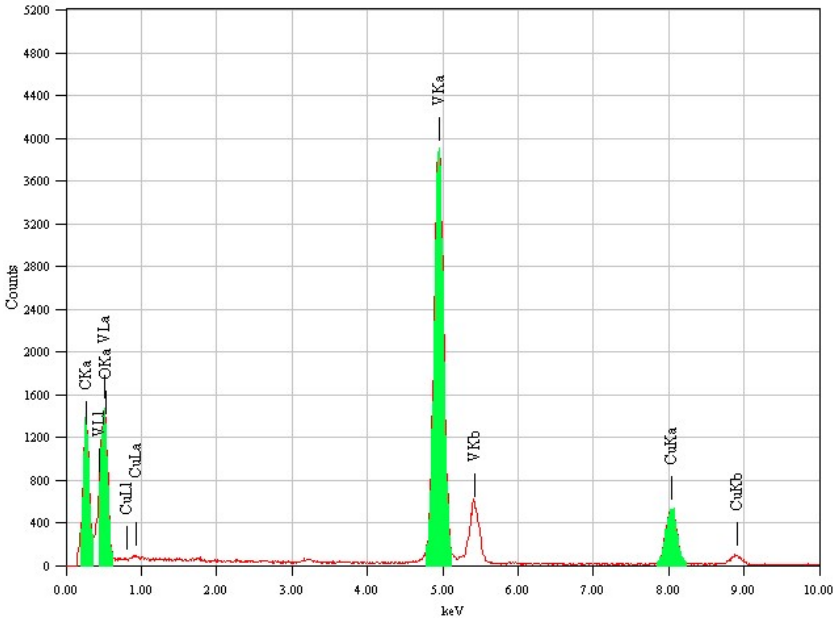

S4. The near edge X-ray absorption fine structure (XANES) spectra

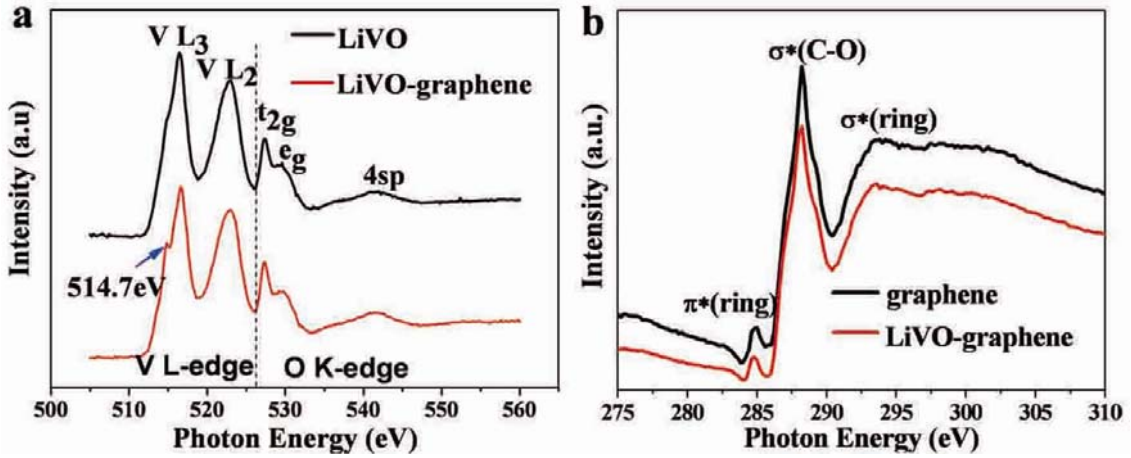

Figure S4 (a) V L-edge and O K-edge NEXAFS spectra, for the as-obtained LiVO-graphene and LiVO, respectively. (b) C K-edge NEXAFS spectra for as-obtained LiVO-graphene and pure graphene, respectively.

The V L-edge NEXAFS spectra represent the d electron-projected unoccupied density of the state, and the O K-edge spectra give the p electron-projected unoccupied density of state of the valence levels. Peaks in the V L-edge region at about 516eV and 522eV in Figure S4a can be assigned to V 2p3/2→3d and V 2p1/2→3d transitions respectively. In the higher energy region, peaks at about 527.4eV and 529.7eV can be contributed to the t_{2g} (527.4eV) and e_g (529.7eV) of V 3d level split by the octahedral crystal field.[4,5] In the C L-edge region of NEXAFS spectra for as-obtained graphene and LiVO-graphene shown in Figure S4b, the peaks at about 284.8eV and 293.5eV contribute to the C-C π* and C-C σ* transitions, respectively. And the peak at about 288.2eV is assigned to the C-O σ* transition.[6]

The peaks in the C L-edge region of NEXAFS spectra for graphene and LiVO-graphene remain unchanged after intercalation, confirming the integrity of the graphene framework during the intercalation process. The peaks at the O K-edge and V L-edge for LiVO and LiVO-graphene are almost the same except in that a small shoulder peaked at 514.7eV which can be ascribed to V^{3+}. All the above information lead us a reasonable conclusion that part of the C-OH functional groups in the graphene form weak C-O-H-O-V bonding while react with part of the O atoms at the bottom of the VO tetragonal pyramid in the intercalation process, part of the electrons transfer from graphene to the neighboring V atoms through the bridging O atoms, which may be the origin of the appearance of V^{3+} in the LiVO-graphene.

S5. The Raman spectroscopy of the as-obtained graphene

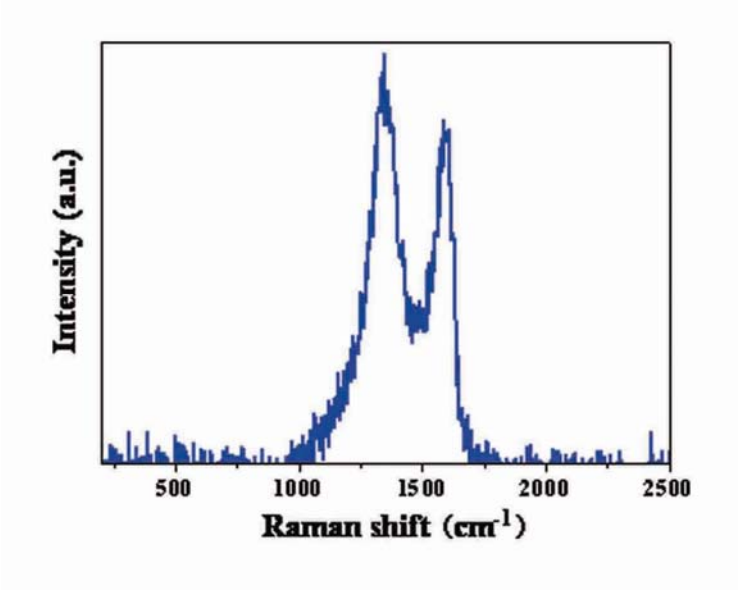

Figure S5. Raman spectroscopy for the as-obtained graphene

Raman spectroscopy was measured to characterize graphene. The Raman spectra of graphene consists a set of distinct peaks including the G peak located at ~1580 cm^{-1}, which dues to the degenerate zone center E_{2g} mode and second-order zone boundary phonons, respectively, and the D peak, which located at ~1350 cm^{-1} due to first-order zone boundary phonons, absent from defect-free graphene, but exists in defected graphene.[8] The as-obtained defective graphene makes it's easy to break the large and thick graphene into small and thin pieces under ultrasonic treatment, which is important for the in situ synthesis of LiVO layer along the existed graphene layer in the intercalated nanosheets.

S6. Exfoliation efficiency comparison of LiVO-graphene in various solvents

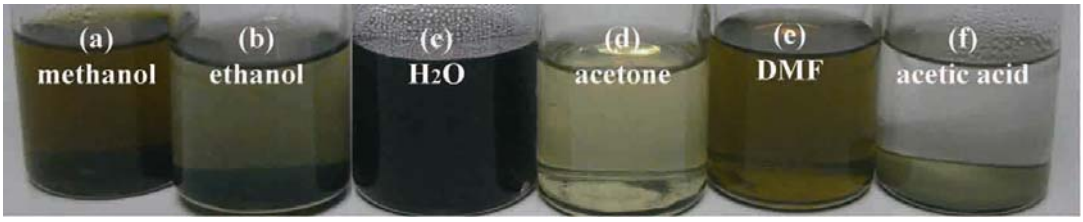

Figure S6. The digital photograph of the LiVO-graphene dispersed in different solvents.

In order to compare the exfoliation efficiency of LiVO-graphene between various solvents, the sample of bulk LiVO-graphene was studied under the following conditions: 10 mg of LiVO-graphene was dispersed in 10ml different solvents and ultrasonicated for 10 minutes. Then all dispersions were allowed to stand still for 3 days. The tested solvents were (a) methanol (b) ethanol (c) H_2O (d) acetone (e) N,N-dimethylfomamide (DMF) and (f) acetic acid. According to the result shown in the photograph, H_2O have the best exfoliation efficiency and is capable of keeping the LiVO-graphene solution stable for a long period of time.

S7. AFM images for the exfoliated nanosheets

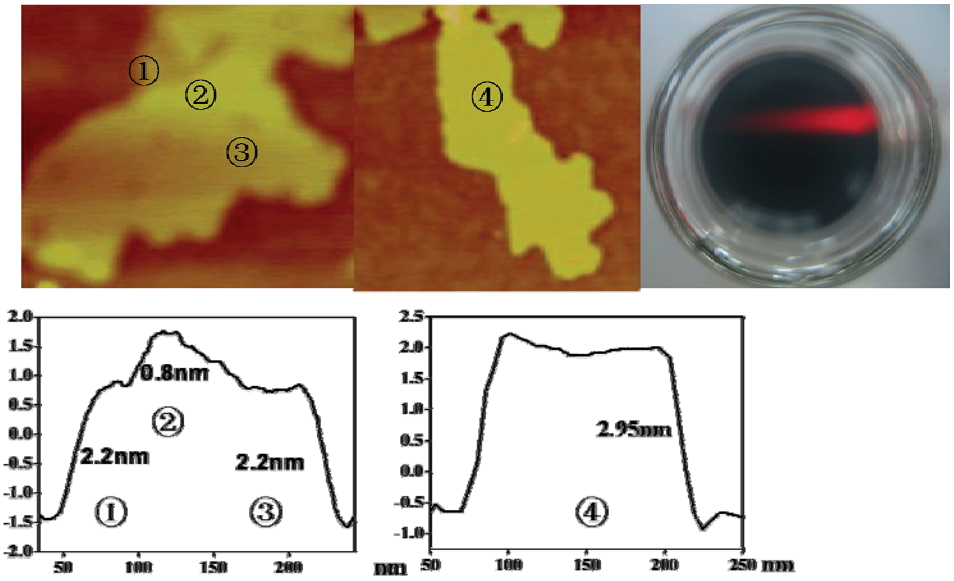

Figure S7: AFM image of the exfoliated LiVO-graphene nanosheets, the relevant thickness of the individual nanosheet labeled by numbers ①-④, and Tyndall effect in the translucent suspension of LiVO-graphene.

S8. Calculationof initial position for graphene layer in LiVO-graphene.

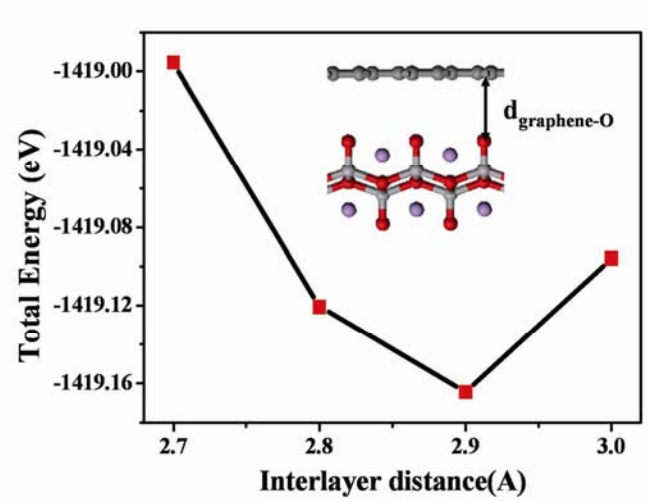

Figure S8**:** The total energy as a function of the initial vertical distance between graphene and O atoms ($d_{graphene-O}$) diagram in LiVO-graphene. The accurate position of the intercalated graphene layer can be estimated by calculating the total energy with different vertical graphene-O distance ($d_{graphene-O}$, Figure 2a), revealing that the equilibrium distance of $d_{graphene-O}$ is 2.9 Å.

S9. DOS of LiVO layer in LiVO-graphene with different position of the embedded Li ions

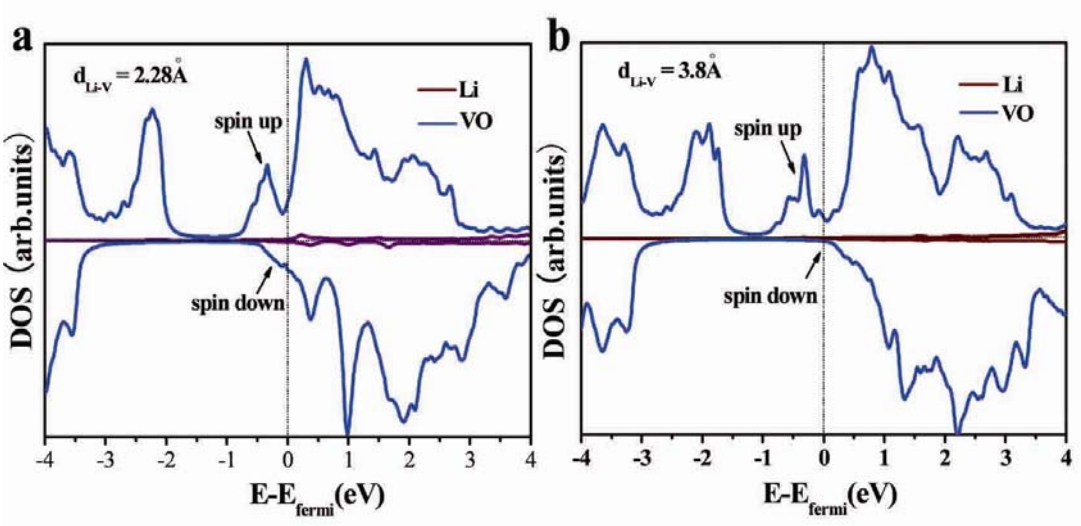

Figure S9: The densities of states (DOS) of LiVO layer in LiVO-graphene with different position of the embedded Li ions: a) d_{Li-V} =2.28Å, b) d_{Li-V} =3.8Å, respectively.

DOS calculations of LiVO layer in LiVO-graphene with different position of the embedded Li ions reveal that the_ LiVO layer is n-type carrier with different position of the embedded Li ions, since the Fermi energy level (E_{fermi}) always lies in the conduction band of LiVO layer.

S10: The transport property of the possible graphene-LiVO-graphene and LiVO-graphene-LiVO nanosheets in the demo transistor.

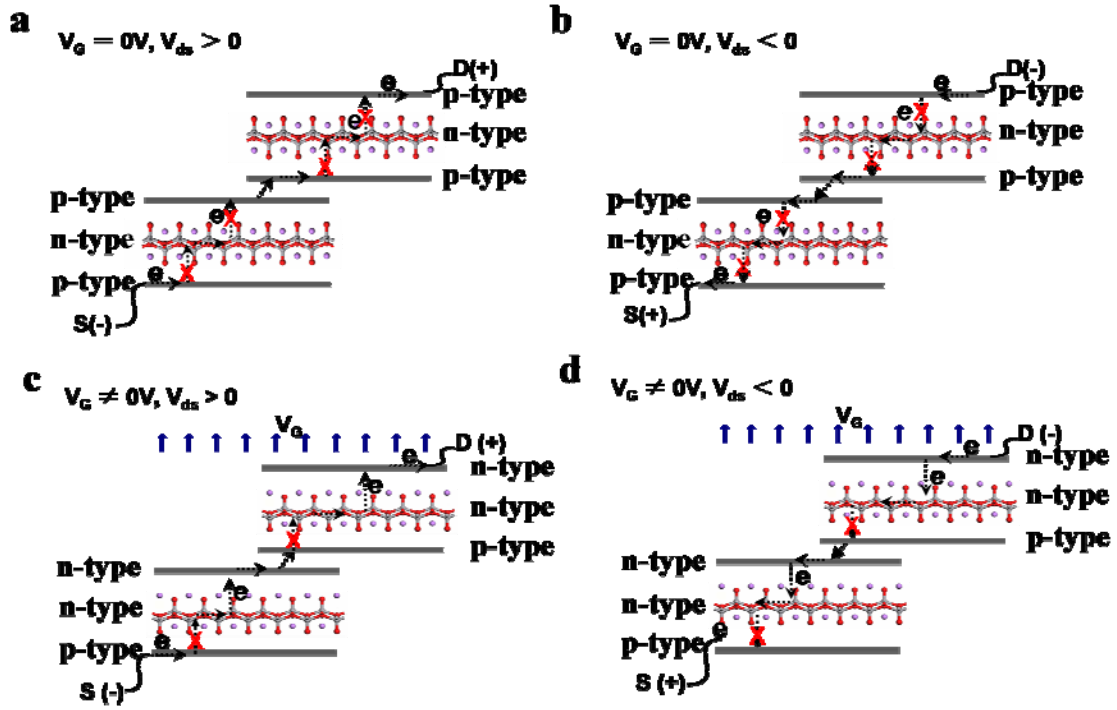

Figure S10-1: The transport property of the possible graphene-LiVO-graphene nanosheets in the demo transistor.

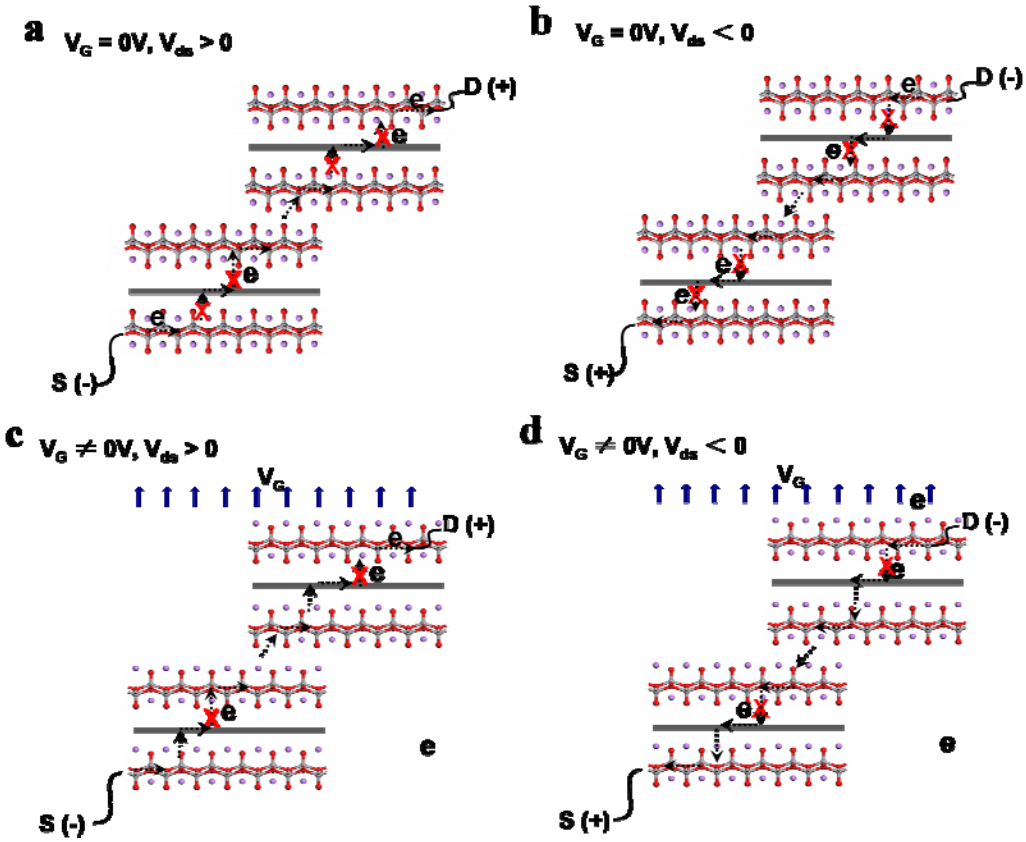

Figure S10-2: The transport property of the possible LiVO-graphene-LiVO nanosheets in the demo transistor.

When there is no external electric field, the graphene layer is always p-type carrier, electrons cannot transfer smoothly due to the inner p-n junction (Figure S10-1a and S10-1b). When an external electric field is added to the nanosheets, the embedded Li ions are pushed near to one of the graphene layer, thus one of the graphene layers in the graphene-LiVO-graphene nanosheets is n-type carrier and the other graphene layer is p-type carrier, electrons cannot transfer smoothly too (Figure S10-1c and S10-1d). So there comes the conclusion that, whether external electric field exists or not, the current perpendicular to the nanosheets is interrupted due to the inner p-n junctions (marked in red X). So the possible graphene-LiVO-graphene nanosheets do not contribute on the transport property of the transistor, even if there may possibly exist some nanosheets with the composition of graphene-LiVO-graphene. The same conclusion can also be given in the case of possible LiVO-graphene-LiVO nanosheets as shown in Figure S10-2: when there is no external electric field, the p-n junction exists all the time (Figure S10-2a and S10-2b); when there exists the external

electric field, the embedded Li ions are pushed to one side of the graphene layer, so electrons can transfer smoothly from LiVO layer to the one side of the graphene layer, but in the other side of graphene layer, Li ions are located far from the graphene layer, electrons cannot transfer freely (Figure S10-2c and S10-2d). So despite the possible existence of the LiVO-graphene-LiVO and graphene-LiVO-graphene nanosheets in the exfoliated nanosheets product, neither of them contributes to the transport property of the transistor, since the electronic channels would be cut off no matter the existence of external electric field in these cases.

S11: The transport property of the LiVO-graphene nanosheets with different overlapping manner in the demo transistor.

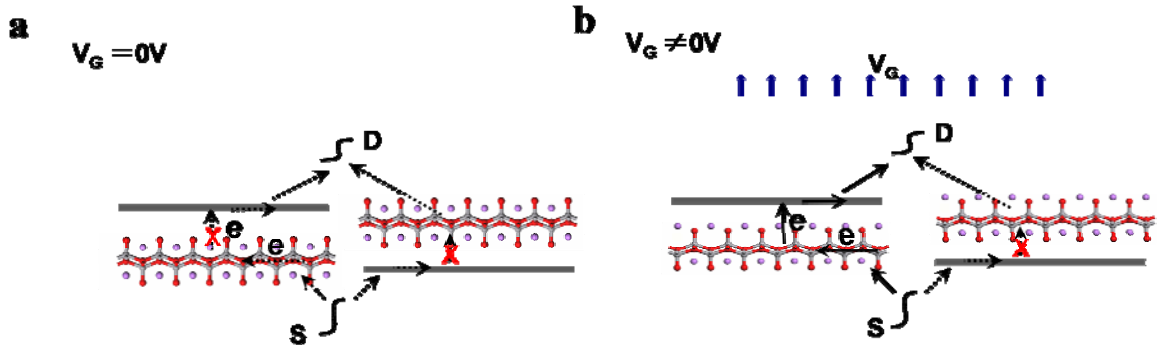

Figure S11: The transport property of the LiVO-graphene nanosheets with different stacking direction in the demo transistor.

To further interpret the influence of the overlapping manners to the transport property of the transistor in detail, here nanosheets with the opposite stacking direction (shown in Figure S11) are brought forward to coexist with the nanosheets with the same stacking direction (as shown in Figure 4b). Now the transport property in this case can be evaluated: If there is no external electric field perpendicular to the nanosheets, the graphene layer is always p-type carrier as shown in Figure S11a**.** If there is the external electric field perpendicular to the nanosheets, the graphene layer (presented in right part of Figure S11b) is p-type carrier because the embedded Li ions are far from the graphene layer, and electrons cannot transfer smoothly between graphene layer and the LiVO layer. While the graphene layer in the left part of Figure S11b is n-type carrier, the embedded Li ions are pushed near to the graphene layer, so electrons flow can transfer freely only from nanosheets with the same stacking direction (as shown in Figure 4b), and nanosheets with the opposite stacking direction do not contribute to the transistor due to the inner p-n junction (Figure S11b). So there comes the conclusion that

even if there may probably coexist the nanosheets with opposite stacking direction, only one assembly manner with the same stacking direction works on the transistor, meanwhile the other assembly manner with opposite stacking direction does not contribute to the transport property of the transistor, since the electronic channels would be cut off no matter the existence of external electric field in this case.

S12: Assembly of LiVO-graphene nanosheets into demo transistor

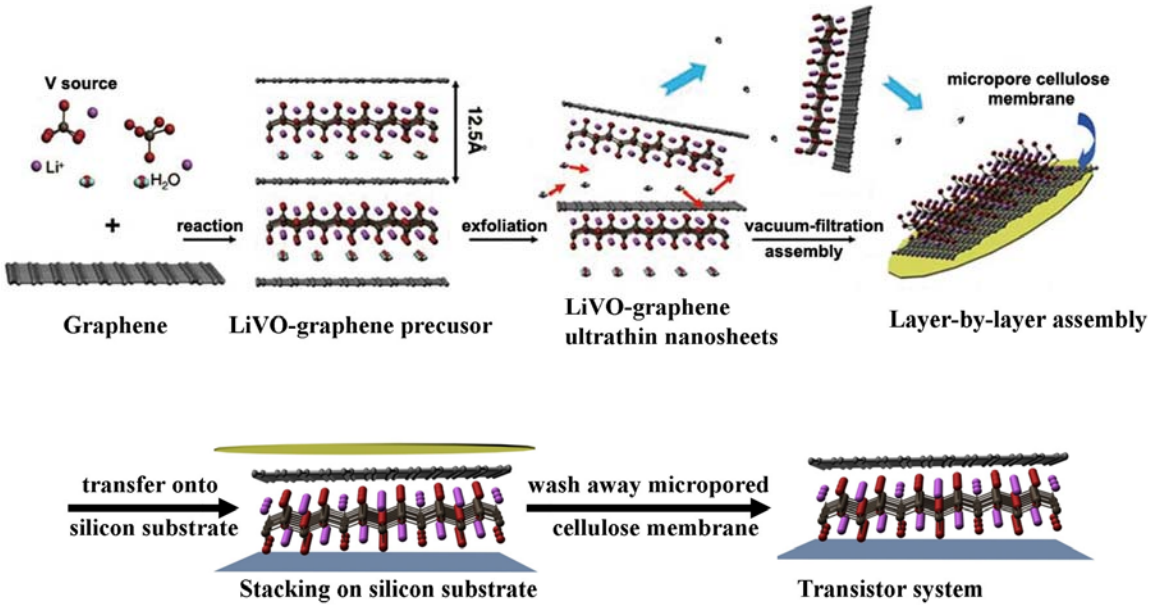

Figure S12: The sketch map of the chemical reaction, exfoliation (promoted by H_2O) process of LiVO-graphene nanosheets, the followed transferring onto silicon substrate, and the device fabrication process.

Reference in the Supporting Information

1. Chirayil, T., Zavalij, P. & Whittingham, M. S. Hydrothermal synthesis and characterization of "$Li_xV_{2-\delta}O_{4-\delta}H_2O$". *Solid State Ionics* **84,** 163 (1996).

2. Zhang, H. T., Gui, Z., Fan, R. & Chen, X. H. Hydrothermal synthesis and characterization of nanorods "$Li_xV_{2-\delta}O_{4-\delta}H_2O$". *Inorg. Chem. Comm.* **5,** 399 (2002).

3. Swiatowska-Mrowiecka, J., Diesbach, S. D. & Maurice, V. Li-Ion Intercalation in Thermal Oxide Thin Films of MoO3 as Studied by XPS, RBS, and NRA. *J. Phys. Chem. C*. **112,** 11050 (2008).

4. Ruzmetov, D., Senanayake, S. D. & Ramanathan, S. X-ray absorption spectroscopy of vanadium dioxide thin films across the phase-transition boundary. *Phys. Rev. B*. **75,** 195102 (2007).

5. Ruzmetov, D., Senanayake,S. D., Narayanamurti, V. & Ramanathan, S. Correlation between metal-insulator transition characteristics and electronic structure changes in vanadium oxide thin films. *Phys. Rev. B*. **77,** 195442 (2008).

6. Zhang, L. S. *et al*. Characterization of partially reduced graphene oxide as room temperature sensor for H_2. *Nanoscale* **3,** 2458 (2011).

7. Ferrari, A. C. *et al*. Raman Spectrum of Graphene and Graphene Layers. *Phy. Rev. Lett.* **97,** 187401(2006).